A New Approach for Accurate Prediction of Subharmonic Oscillation in Switching Regulators–Part I: Mathematical derivations

A. El Aroudi, *Senior Member, IEEE*

***Abstract*—This part of the paper takes a new look at the stability of the fundamental periodic behavior and the associated subharmonic oscillation boundary in dc-dc switching regulators with fixed frequency pulse width modulation. After revisiting different approaches applied to a unified reduced-order model of switching regulators, the work presents a novel way of obtaining such a boundary without any simplification nor order-reduction. A new simple closed-form condition is then obtained using the new approach which is valid for different strategies with both trailing edge and leading edge modulation schemes. The critical condition is obtained from the steady-state response using an asymptotic approach without resorting to frequency-domain Fourier analysis or using the monodromy or the Jacobian matrix of the discrete-time model. Unlike the method based on the Fourier series expansion, the proposed method does not require the use of any transform and, most importantly, can be applied to bilinear switching regulators. As a byproduct of the proposed method, a singularity problem that is encountered in steady-state, when the system involves integrators in the feedback loop, is addressed and a solution is developed to achieve a closed-form expression in the presence of such integrating feedback loops.**

***Index Terms*—Circuit stability, DC-DC power conversion, Bifurcation, Bilinear systems, Nonlinear systems, Power electronics, Switched mode power supplies, Time domain analysis.**

I. Introduction

SWITCHING regulators are widely used for power sources and power management systems in different applications such as in portable devices, solid-state lighting drivers and technologies for renewable energy production such as in PV systems. However, despite their engineering use, one of their main drawbacks is their inherent nonlinearity making them prone to exhibit a large variety of complex dynamics and undesired behaviors under parameter changes. For instance, subharmonic oscillation in dc-dc switching regulators has been well documented in the early 80's [1]. Since then, its prediction has been widely explored [2], [3]. However, most of the used models simplify the regulator as a first-order system, hence allowing to derive a simple closed-form expression to predict the subharmonic instability boundary. Assuming a triangular (piecewise linear) inductor current, and based on the analysis of how a perturbation of this current propagates within a switching cycle, a slope-based criterion can be obtained establishing that the boundary of subharmonic oscillation in a switching converter under peak/valley Current Mode Control (CMC) is given by [4]–[6]:

$$-\frac{m_0+m_a}{m_1+m_a}=1 \tag{1}$$

which can conveniently be rewritten as follows [7]:

$$m_a=-\frac{1}{2}(m_1+m_0):=m_{a,\mathrm{cri}} \tag{2}$$

where $m_1>0$ and $m_0<0$ are the slopes of the control signal during the charging (ON) and discharging (OFF) phases respectively and $m_a>0$ is the slope of the ramp compensator. For stability, the ramp slope m_a must be greater than a certain critical value $m_{a,\mathrm{cri}}$ given by (2).

The previous equivalent critical conditions are only valid for the inner CMC loop while ignoring any effect of the outer voltage feedback and they fail short in predicting subharmonic oscillation in the case of CMC with voltage loop closed [3] because in the process of their derivation the ripple of the output voltage and the corresponding feedback signal is completely ignored. These conditions also fail for a conventional Voltage Mode Control (VMC) and average CMC because the control signal waveform in this case is not triangular [8], [9].

Some early results concerning stability conditions for constant switching frequency power converters under CMC, taking into account the interaction of the current and voltage feedback loops, have been first derived in [1] and later in [10]. In an attempt to predict this phenomenon with small-signal frequency domain models, an approach has been proposed in [3] consisting of augmenting the dimension of the averaged model by taking into account the sampling effects. Other more advanced small-signal models and their equivalent circuit representations are also proposed in [11] based on a linearized describing function method extending the results obtained in peak CMC to average CMC. Recent results based on the same method proved that the approach of [3] still fail short in predicting the behavior of ripple-based controlled converters that use the output voltage in the fast loop [12], [13]. Taking support from a bifurcation analysis approach, the prediction of subharmonic oscillation has been mainly based on deriving an accurate discrete-time model and then linearizing it in the vicinity of the operating point. This approach has been used

A. El Aroudi is with the GAEI research center, Departament d'Enginyeria Electrònica, Elèctrica i Automàtica, Escola Tècnica Superior d'Enginyeria, Universitat Rovira i Virgili, 43007, Tarragona, Spain (e-mail:abdelali.elaroudi@urv.cat).

This work was supported by the Spanish *ministerio de Economía y Competitividad* under grant DPI2013-47437-R.

Color versions of one or more of the figures in this paper are available online at http://ieeexplore.ieee.org

since the pioneering works in the 90's and 00's [14]–[26]. It has been demonstrated that similar results can be obtained by using Floquet theory combined with Filippov's method and the associated monodromy matrix [27]–[29].

Due to the importance of its prediction from both theoretical and practical points of view, this phenomenon is receiving increasingly more attention from many researchers [26], [29]–[34]. Using discrete-time modeling and Filippov method, it was demonstrated recently in [29] that the approach based on the describing function models [11] is inaccurate for predicting subharmonic oscillation in switching converters under V^2 and V^2I_C VMC strategies. Improved averaged models have also been developed to approximately and numerically predict the onset of this phenomenon in power electronics circuits [13], [26], [35]. Nevertheless, to determine *accurately*, the boundary of subharmonic oscillation in switching converters, appropriate analytical methods are required. Determining analytically the boundary by this procedure does not appear simple. The analytical determination of this boundary can be tackled from several points of view. Roughly speaking, it can be determined either by:

- **A dynamic approach:** It consists first of deriving a nonlinear model of the closed loop system, obtaining the operating point, linearizing the model in the vicinity of this point hence getting either the Jacobian matrix $\mathbf{J}$ or an equivalent transfer function in the z-domain and tracking the movements of the roots of the characteristic equation evaluated at the steady-state operating point. The critical boundary condition can be derived by imposing the corresponding singularity in the characteristic equation $\det(\mathbf{J}-\lambda\mathbf{I})=0$. Namely, at the subharmonic oscillation boundary, one of the eigenvalues is equal to -1 and hence the critical boundary condition is simply $\det(\mathbf{J}+\mathbf{I})=0$. Algebraic manipulation of the previous equation leads to a closed-form expression in terms of the system state-space model matrices. This procedure has been first used in [36] and recently in [32].
- **A static approach:** It consists of analyzing the steady-state response in the subharmonic regime. This approach was first used in [36], [37] and recently in a series of papers by the same author [33], [34], [38] and also in [8]. The feedback signal is first expanded as a Fourier series and the switching conditions, are then used. With that approach an effort to transform the results from the Fourier frequency-domain into the time-domain must be done. In [33], [34], [38], this transformation was performed based on elementary partial fraction decomposition of the system *linear loop gain* after defining some elementary cases in the Laplace $s-$domain and listing them in the form of tables hence finally obtaining a more general condition than (2). In [8], some well-known Fourier series properties have been used to transform the condition for subharmonic oscillation occurrence expressed in terms of the system linear loop gain from the Fourier frequency-domain to a matrix-form time-domain condition. The approach in [8], [33], [34], [38] is only applicable for those converters that can be formulated in the form of a *linear system* subject to a periodic excitation generated by the PWM process. Nevertheless, this kind of representation is the exception rather than the rule in switching converters. It is a well known fact that the state-space model of the wide class of dc-dc switching converters such as boost, buck-boost, Čuk, SEPIC, flyback and many others are described by *bilinear* models which include the product of the driving signal and the state vector. *We will see in this paper that a steady-state analysis of the solution in the time-domain can be applied in general to both* linear *and* bilinear *converters. A new expression for the stability boundary will be obtained without need to use the Fourier series expansion and without having to perform any transformation nor needing the calculation of the Jacobian or the monodromy matrix.*

The accurate steady-state approach used and the closed-form expression derived have the following advantages:

1) *General:* No matter how complicated the topology of the circuit is, the same expression applies whenever the system has two switching configurations. The approach is therefore very general and might be applied to many examples of switching converters with both linear and bilinear power stages.
2) *Simple:* The closed-form stability condition contains only the state transition matrices of the two configurations of the switched converter, the state velocities (vector fields) evaluated at the operating point and the vector of feedback coefficients.
3) *Direct:* The expression is derived directly in the time-domain without needing any transform.
4) *Unified:* The expressions can be applied to different constant frequency PWM strategies with both Trailing Edge Modulation (TEM) and Leading Edge Modulation (LEM) schemes such as peak CMC, valley CMC, average CMC, and the recent schemes V^1 VMC [39], I^2 CMC (like a PI CMC) [40], [41], V^2 VMC and V^2I_C control [29], among others.
5) *Powerful:* The effect of the main and the parasitic parameters can all be considered with little difficulty. In particular, the effect of the integral action used in many control schemes is explicitly revealed.

The rest of the paper is organized as follows. Section II presents the general full-order model of fixed frequency dc-dc switching regulators. In section III, a simplified reduced-order model is derived by considering the feedback signal the only state variable of the system. Using this model, section III also revisits different dynamic approaches, both in the time and in the frequency domains, to *approximately* predict subharmonic oscillation in switching regulators under fixed switching frequency control schemes. In section IV , it is shown that the stability boundary in (1) or equivalently (2) can be obtained by just performing a steady-state analysis either in the frequency domain or in the time domain. A general unified approach for *accurate* prediction of subharmonic oscillation is presented in Section V extending the results of sections III and IV to *bilinear* converters without any simplification nor order-reduction. A new exact and simple closed-form expression

TABLE I
THE INPUT AND THE OUTPUT VOLTAGES FOR THE THREE ELEMENTARY SWITCHING CONVERTERS [42].

	Buck	**Boost**	**Buck-Boost**
Input voltage	$v_{\rm ap}$	$v_{\rm ca}$	$v_{\rm ac}$
Output voltage	$v_{\rm cp}$	$v_{\rm pa}$	$v_{\rm pc}$

for predicting subharmonic oscillation is then obtained from this approach. Finally some concluding remarks and possible extensions of this work are summarized in the last section.

II. MODELING OF CLOSED LOOP SWITCHING REGULATORS

A. A unified system description and its full-order bilinear continuous-time model

Switching regulators comprise three elements: a power stage to be controlled, a controller and a pulse width modulator/compensator. The three elements are linked by a single feedback loop in VMC and *generally* by two loops in CMC. Fig. 1 shows the unified three-terminal circuit diagram of elementary switching converters buck, boost and buck-boost under PWM fixed frequency VMC and CMC strategies. The terminals designations a, p, and c in Fig. 1 refer to active, passive and common respectively [42]. The common node between the switches S and $\overline{\rm S}$ connects to the inductor whose inductance is L. The switching element $\overline{\rm S}$ is a diode in unidirectional converters while it is a transistor in bidirectional and synchronous converters. Table I shows the input and the output voltages for the three elementary converters in terms of the voltage between the terminals a, p, and c. Other high-order converters such as Čuk and SEPIC can be represented by the same circuit diagram after adding the pertinent filtering components. Depending on the application, either the input or the output (voltage or current) is the variable that must be controlled. In conventional applications of switching converters, the voltage to be controlled is the output voltage. However, in some applications such as in renewable energy PV systems, the variable to be controlled is the input voltage while the output voltage is considered constant [43]. In LED driving applications, the output current must be controlled [44], [45].

The system consisting of the power stage and the controller can be described by a piecewise linear switched model. To facilitate the state-space representation of the system, two vectors are used: the state vector $\mathbf{x}$ and the input vector $\mathbf{w}$. The vectors are represented by boldface lower case letters and they are column vector in general. When a row vector is needed, the transpose operator $^{\intercal}$ is applied to its corresponding column vector. The matrices are boldface upper case. The dynamics of a switching regulator is described by a state-space model that can be written in the following form:

$$\dot{\mathbf{x}}(t) = \mathbf{A}_1\mathbf{x}(t)+\mathbf{B}_1\mathbf{w}, \quad \text{for} \quad u=1, \tag{3a}$$

$$\dot{\mathbf{x}}(t) = \mathbf{A}_0\mathbf{x}(t)+\mathbf{B}_0\mathbf{w}, \quad \text{for} \quad u=0, \tag{3b}$$

$$\dot{x}_i(t) = e(t). \tag{3c}$$

where $\mathbf{A}_0 \in \mathbb{R}^{N\times N}$, $\mathbf{A}_1 \in \mathbb{R}^{N\times N}$, $\mathbf{B}_0 \in \mathbb{R}^{N\times p}$ and $\mathbf{B}_1 \in \mathbb{R}^{N\times p}$ are the system state matrices and $\mathbf{w} \in \mathbb{R}^p$ is the vector of the external parameters of the plant and/or the controller supposed to be constant within a switching cycle. The signal u in the model (3a)-(3c) is the binary signal which is generated by the PWM process and applied to the main switch S. The variable x_i in (3c) stands for the integral of the sensed outer voltage error e in both VMC and CMC with voltage loop closed but it can also represent the integral of the sensed inner current error in CMC with voltage loop open. This variable was deliberately separated from the rest of state variables to start with a *well-posed* problem[1] and to avoid some matrix singularities appearing in the expressions of the system trajectories and their steady-state values at the switching time instants [9], [32]. It should be noted that in [32] different examples of switching converters were considered but the problem is mathematically *ill-posed* for those examples involving an integrator in the feedback loop. Note, for instance, that if the variable x_i is included within the state vector $\mathbf{x}$, the inverse matrices $\mathbf{A}_1^{-1}$ and $\mathbf{A}_0^{-1}$ needed for calculating the system state trajectories during a switching cycle will not exist. In [32] and in a series of other works by the same author of [32], to avoid such an *ill-posedness* problem, the integrator dynamics is modified by converting it to a low pass filter with a sufficiently small non-zero pole replacing the pole at zero of the integrator. However, choosing an inappropriate value of this parameter could give rise to serious numerical artifacts. Moreover, with that approach the effect of the integrator is hidden within the complete state-space representation. Here, the nature of the integrator is maintained and its effect will be clearly revealed. More details about other related matrix singularities will be given in Section V.

The full-order switched model of a switching converter as given in (3a)-(3c) can also be expressed as follows:

$$\dot{\mathbf{x}}(t) = \mathbf{m}_0(\mathbf{x}(t)) + (\mathbf{m}_1(\mathbf{x}(t)) - \mathbf{m}_0(\mathbf{x}(t)))u(t), \tag{4a}$$

$$\dot{x}_i(t) = e(t). \tag{4b}$$

where $\mathbf{m}_1(\mathbf{x}(t)) = \mathbf{A}_1\mathbf{x}(t)+\mathbf{B}_1\mathbf{w}$ and $\mathbf{m}_0(\mathbf{x}(t)) = \mathbf{A}_0\mathbf{x}(t)+\mathbf{B}_0\mathbf{w}$ are the state velocities (or vector fields) for $u=1$ and $u=0$ respectively. It is worth noting that, generally, the previous model is *bilinear* unless the term $\mathbf{m}_1(\mathbf{x})-\mathbf{m}_0(\mathbf{x})$ multiplying the driving signal u is independent on the state $\mathbf{x}$. Although strictly speaking, this is only the case of the ideal buck converter, it is also an approximate representation of most switching converters under some specific conditions [46].

B. Modeling the pulse width modulator

The driving signal u of the main switch S is the result of comparing cyclically a control signal $v_{\rm con}$ depending on the state variables and a $T-$periodic ramp signal $v_{\rm ramp}$ together with additional logic rules dictated by an SR latch and a clock signal to force a single switching per cycle. Some VMC implementations do not use a latch but the approach presented here is still valid for these cases provided that the $T-$periodic orbit is characterized by one and only one switching within the period T. In TEM strategies, the state of the main switch S is forced to be ON ($u=1$) at the beginning of each switching

[1] A mathematical problem is *well posed* if a solution exists and is unique.

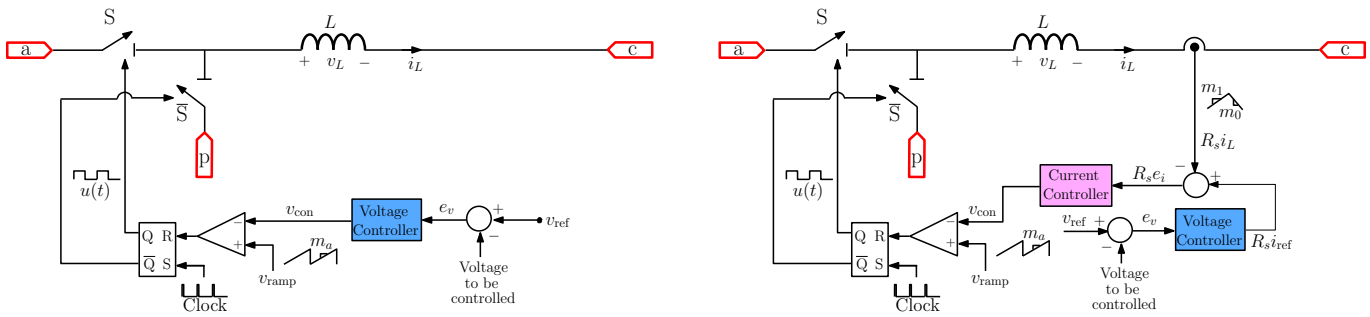

(a) VMC (b) CMC

Fig. 1. Circuit diagrams of a switching converter under (a) VMC and (b) CMC. The voltage and/or the current controllers can be static or dynamic.

period and it is turned OFF ($u = 0$) whenever the control signal $v_{\rm con}$ and the ramp signal $v_{\rm ramp}$ intersect. The state of $\overline{\rm S}$ is complementary to that of S. The previous logic is inverted in LEM strategies. The main assumption in the approach of this paper is that the converter is working in Continuous Conduction Mode (CCM) with two switching configurations. The switching condition that completes the model given in (3a)-(3c) or equivalently (4a)-(4b) can be expressed as follows:

$$v_{\rm con}(t) = v_{\rm ramp}(t). \tag{5}$$

where $v_{\rm ramp}$ is the ramp signal that can be expressed by:

$$v_{\rm ramp}(t) = V_l + m_a(t \bmod T), \tag{6}$$

where V_l is its lower value, $m_a = V_M/T$ is its slope, V_M is its amplitude and T is its period. The ramp voltage is used either for modulation or for slope compensation. For instance, in conventional VMC, the ramp voltage is used for modulation. In peak CMC, it is used for slope compensation which can be achieved either by subtracting this signal from the reference signal $R_s i_{\rm ref}$ or by adding it directly to the voltage $R_s i_L$ representing the sensed inductor current. Note that both schemes are mathematically equivalent to the one represented in Fig. 1-b in which the the ramp signal is compared with the output of the current controller. The scheme in Fig. 1-b is preferred because dynamic controllers for the inductor current such as average CMC can also be covered. When the ramp is not used, the approach is still valid by just making $v_{\rm ramp}(t) = 0$ in (5). Let us focus our study on TEM strategies. Hence, the duty cycle d_n of the signal u, at the switching cycle $(nT, (n+1)T)$, $(n \in \mathbb{N})$, is dictated cyclically by the following switching condition:

$$v_{\rm con}(d_n T) = V_l + m_a(d_n T \bmod T). \tag{7}$$

In order to cover different static and dynamic cases of VMC and CMC, let us express the control signal as $v_{\rm con} = v_r - \mathbf{K}^\intercal \mathbf{x} + W_i x_i$, where v_r is a constant and $\mathbf{K}^\intercal$ is a feedback vector depending on the control mode used to be specified for each case. Hence, the switching condition (7) becomes:

$$v_r - \mathbf{K}^\intercal \mathbf{x}(d_n T) + W_i x_i(d_n T) = V_l + m_a(d_n T \bmod T). \tag{8}$$

which can be equivalently written in the following form:

$$\underbrace{\mathbf{K}^\intercal \mathbf{x}(d_n T) - W_i x_i}_{y(d_n T)} = \underbrace{(\rho - m_a(d_n T \bmod T))}_{r(d_n T)}. \tag{9}$$

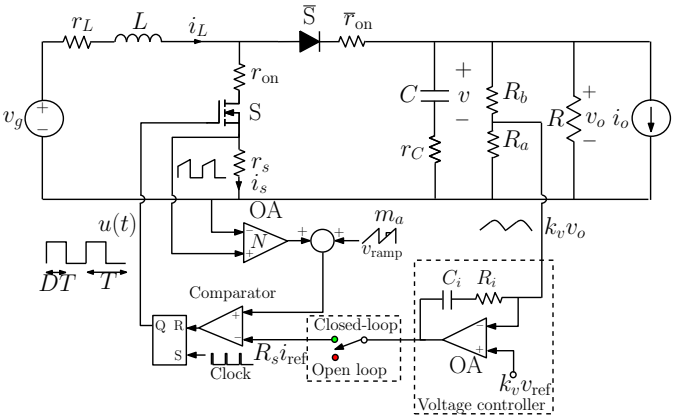

Fig. 2. A boost converter under a peak CMC with voltage loop open or closed using a PI controller.

where $\rho = v_r - V_l$. Therefore, the system switches from the ON phase ($u = 1$) to the OFF phase ($u = 0$) at the switching instant $d_n T$ decided by (9) which can be expressed as follows:

$$y(d_n T) = r(d_n T). \tag{10}$$

To make the presentation more clear and to specify ρ, $\mathbf{K}^\intercal$ and W_i, let us consider, in the next subsections, two different examples. Note that once these parameters are specified, the variables y and r can be determined according to (9).

C. Example 1: A boost converter under a peak CMC

Consider the boost converter under CMC depicted in Fig. 2 [47]. By applying KVL to the power stage we obtain the following equations:

$$\frac{{\rm d}v}{{\rm d}t} = -\frac{\alpha v}{RC} + \frac{\alpha i_L}{C}(1-u) - \frac{i_o}{C}, \tag{11a}$$

$$\frac{{\rm d}i_L}{{\rm d}t} = -\frac{\alpha v}{L}(1-u) - \left(\frac{r_1}{L}u + \frac{r_0}{L}(1-u)\right) i_L + \frac{v_g}{L}, \tag{11b}$$

where, $r_1 = r_L + r_s + r_{\rm on} + \alpha r_C$, $r_0 = r_L + \overline{r}_{\rm on} + \alpha r_C$, $\alpha = R/(R+r_C)$, R is the load resistance and r_C is the equivalent series resistance (ESR) of the output capacitor whose capacitance is C. Note that with an ideal capacitor, $r_C = 0$, then $\alpha = 1$ and $v_o = v$. The parameters $r_{\rm on}$ and $\overline{r}_{\rm on}$ are the ON resistances of the switches S and $\overline{\rm S}$ respectively while r_s is a small shunt resistance used for current sensing. The output

current i_o can represent any load working as a current sink such as, for instance, another downstream converter working under CMC [48], [49]. All the other parameters appearing in the previous model can be identified in the schematic circuit diagram of Fig. 2. In terms of the general description given in (3a)-(3b), the system matrices for this example are as follows:

$$\mathbf{A}_1 = \begin{pmatrix} -\frac{\alpha}{RC} & 0 \\ 0 & -\frac{r_1}{L} \end{pmatrix}, \ \mathbf{B}_1 = \begin{pmatrix} -\frac{1}{C} & 0 \\ 0 & \frac{1}{L} \end{pmatrix}, \quad (12a)$$

$$\mathbf{A}_0 = \begin{pmatrix} -\frac{\alpha}{RC} & \frac{\alpha}{C} \\ -\frac{\alpha}{L} & -\frac{r_0}{L} \end{pmatrix}, \ \mathbf{B}_0 = \mathbf{B}_1, \mathbf{w} = \begin{pmatrix} i_o \\ v_g \end{pmatrix}. \quad (12b)$$

1) Voltage loop open: Let us consider first that the outer voltage loop is open and therefore the current reference $i_{\rm ref}$ is constant. This assumption is widely used to study the stability of the inner current loop by neglecting the ripple at the output of voltage controller [5]. Typically, the switch current i_s is sensed using a small shunt resistance r_s to gather the information about the inductor current i_L. The voltage in the terminals of the shunt resistor is amplified by a voltage amplifier with a gain N and its output gives a voltage $r_sNi_s := R_si_s$, where ($R_s = r_sN$). The switch is turned ON cyclically each switching period T and it is turned OFF whenever $R_si_s + v_{\rm ramp}$ reaches the signal $R_si_{\rm ref}$ or equivalently when R_si_s reaches the signal $R_si_{\rm ref} - v_{\rm ramp}$. Hence, the switching condition can be written as follows:

$$R_si_{\rm ref} - R_si_s(t) = v_{\rm ramp}(t). \quad (13)$$

Without loss of generality, let $V_l = 0$. According to (13), and because during the ON state, the inductor current i_L coincides with the switch current i_s, the duty cycle d_n at the nth switching cycle is determined by the following switching condition:

$$R_si_{\rm ref} - R_si_L(d_nT) = m_a(d_nT \bmod T). \quad (14)$$

which can be adapted as in (9) by selecting $\mathbf{x} = (v, \ i_L)^\intercal$, $v_r = R_si_{\rm ref}$, $\rho = v_r - V_l = R_si_{\rm ref}$, $\mathbf{K}^\intercal = (0, \ R_s)$. Because the current loop does not involve an integrator in this case, the integral variable must be inhibited and $W_i = 0$.

2) Voltage loop closed: In this case, the current reference $i_{\rm ref}$ is provided by the output of the voltage controller. The output voltage in the boost converter of Fig. 2 can be expressed as follows:

$$v_o(t) = \alpha(v(t) + r_Ci_L(t)(1 - u(t))). \quad (15)$$

Note that this voltage is discontinuous when $r_C \neq 0$. The voltage controller function is to compensate the error $k_vv_{\rm ref} - k_vv_o$ detected between a fixed reference voltage level $k_vv_{\rm ref}$ and the sensed output voltage k_vv_o. The voltage sensor gain is implemented by a voltage divider consisting of the resistors R_a and R_b. In this example, the voltage controller is a simple PI regulator with a pole at the origin and a zero ω_{vz}. The controller transfer function can be expressed as follows:

$$H_v(s) = W_i\frac{1 + s/\omega_{vz}}{s}, \quad (16)$$

where W_i is the integrator gain. In terms of the passive components constituting the voltage sensor and controller, the following relationships hold between the parameters:

$$k_v = \frac{R_a}{R_a + R_b}, \ W_i = \frac{1}{R_bC_i}, \ \omega_{vz} = \frac{1}{R_iC_i}. \quad (17)$$

According to the schematic diagram of Fig. 2, when the voltage loop is closed, the current reference (scaled by R_s) $R_si_{\rm ref}$ can be expressed as follows:

$$R_si_{\rm ref}(t) = \frac{k_vW_i}{\omega_{vz}}(v_{\rm ref} - v_o(t)) + k_vW_i\int(v_{\rm ref} - v_o(t))\mathrm{d}t. \quad (18)$$

Let $x_i = \int k_v(v_{\rm ref} - v_o(t))\mathrm{d}t$ and hence the following differential equation is needed to complete the model of the switching regulator:

$$\frac{\mathrm{d}x_i}{\mathrm{d}t} = k_v(v_{\rm ref} - v_o(t)). \quad (19)$$

The reference signal $R_si_{\rm ref}$ can be expressed as follows:

$$R_si_{\rm ref}(t) = \frac{k_vW_i}{\omega_{vz}}(v_{\rm ref} - v_o(t)) + W_ix_i(t). \quad (20)$$

Substituting the output voltage v_o by its expression in (15), the switching condition can be expressed as follows:

$$\frac{k_vW_i}{\omega_{vz}}(v_{\rm ref} - (\alpha(v(t) + r_Ci_L(t)(1 - u)))) + W_ix_i(t) - (R_si_s(t) + v_{\rm ramp}(t)) = 0. \quad (21)$$

The switching from the ON to the OFF state takes place when the following equality holds:

$$\frac{k_vW_i}{\omega_{vz}}(v_{\rm ref} - \alpha v(d_nT)) + W_ix_i(d_nT) - R_si_L(d_nT) - m_a(d_nT \bmod T) = 0, \quad (22)$$

which can also be adapted as in (9) by selecting $\mathbf{x} = (v, \ i_L)^\intercal$, $v_r = W_ik_v/\omega_{vz}v_{\rm ref}$, $\rho = v_r$, $\mathbf{K}^\intercal = (W_ik_v/\omega_{vz}, \ R_s)$. If the controller involves more state variables such as in type-II [4] or type-III [50] compensation schemes, the expression of the switching condition can be adapted by just adding these variables weighted by their corresponding gains.

D. Example 2: A buck converter under a type-III VMC

Fig. 3 shows the circuit diagram of a dc-dc buck converter under VMC with a type-III compensator. The compensation network comprises an error amplifier with the reference voltage $k_vv_{\rm ref}$ on the non-inverting pin and the sensed output k_vv_o from the buck converter on the inverting pin. The voltage sensing is carried out by a simple voltage divider using the resistances R_a and R_b. The activation of the switch S and $\overline{\rm S}$ is carried out as follows: the sensed error voltage $e = k_v(v_{\rm ref} - v_{\rm o})$ is processed by means of the type-III compensator, and the output $v_{\rm con}$ of this compensator is connected to the inverting pin of the comparator whereas a $T-$periodic ramp signal $v_{\rm ramp}$ is applied to the non-inverting pin. The output of the comparator is connected to the reset entry of an SR flip-flop while a $T-$periodic clock synchronized with the ramp signal is connected to its set entry in such a way that the switch S is turned ON (therefore $u = 1$) at the

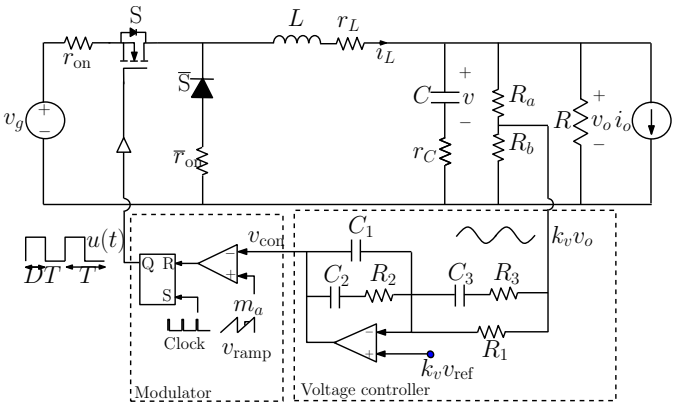

Fig. 3. Schematic circuit diagram of a dc-dc buck converter under VMC with type-III compensator.

starting of each period and it is turned OFF ($u = 0$) whenever $v_{\rm con} = v_{\rm ramp}$. The switch $\overline{\rm S}$ is driven complementarily to S. Let $r_1 = r_{\rm on} + \alpha r_C$ and $r_0 = \overline{r}_{\rm on} + \alpha r_C$. By applying KVL to the power stage we obtain the following equations:

$$\frac{{\rm d}v}{{\rm d}t} = -\alpha\frac{v}{RC} + \frac{\alpha i_L}{C} - \frac{i_o}{C}, \tag{23a}$$

$$\frac{{\rm d}i_L}{{\rm d}t} = -\frac{\alpha v}{L} - (\frac{1}{L}(r_1 u + r_0(1-u)))i_L + \frac{v_g}{L}u, \tag{23b}$$

where $\alpha = R/(R + r_C)$. All the parameters appearing in the previous model can be identified in Fig. 3. The transfer function of a type-III controller can be expressed as follows:

$$H_v(s) = \frac{W_i}{s}\frac{(s/\omega_{z1}+1)(s/\omega_{z2}+1)}{(s/\omega_{p1}+1)(s/\omega_{p2}+1)}. \tag{24}$$

where W_i is the integrator gain, ω_{z1} and ω_{z2} are two zeros and ω_{p1} and ω_{p2} are two poles to be placed appropriately according to the rules detailed in [50]. Namely, the zeros are placed close to the LC resonant frequency of the buck converter power stage, one of the poles is placed at one half of the switching frequency and another pole is placed at the zero caused by the ESR of the output capacitor [50]. The zeros, the poles and the integrator gain are given by the following expressions in terms of the passive elements in the network of Fig. 3:

$$\omega_{z1} = \frac{1}{R_2C_2},\ \omega_{z2} = \frac{1}{(R_1+R_3)C_3}, \omega_{p1} = \frac{C_1+C_2}{R_2C_1C_2},$$
$$\omega_{p2} = \frac{1}{R_3C_3},\ W_i = \frac{1}{R_1(C_1+C_2)}. \tag{25}$$

Performing a partial fraction decomposition on (24), it can be rewritten in the following form:

$$H_v(s) = \frac{W_i}{s} + \frac{W_{p1}}{s+\omega_{p1}} + \frac{W_{p2}}{s+\omega_{p2}}, \tag{26}$$

where W_{p1} and W_{p2} are feedback coefficients corresponding to the state variables v_{p1} and v_{p2} of the controller. These coefficients can be expressed as follows:

$$W_{p1} = \frac{W_i\omega_{p2}(\omega_{z1}\omega_{z2} - \omega_{p1}(\omega_{z1}+\omega_{z2}) + \omega_{p1}^2)}{\omega_{z1}\omega_{z2}(\omega_{p1}-\omega_{p2})}, \tag{27a}$$

$$W_{p2} = -\frac{W_i\omega_{p1}(\omega_{z1}\omega_{z2} - \omega_{p2}(\omega_{z1}+\omega_{z2}) + \omega_{p2}^2)}{\omega_{z1}\omega_{z2}(\omega_{p1}-\omega_{p2})}. \tag{27b}$$

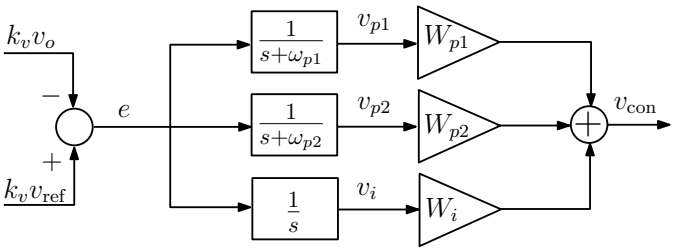

Fig. 4. An equivalent block diagram of a type-III compensator.

Fig. 4 shows an equivalent block diagram of a type-III compensation network according to the partial fraction decomposition of (26). The state variables v_{p1} and v_{p2} of the controller are shown in the same figure. Let $\mathbf{x} = (v,\ i_L, v_{p1},\ v_{p2})^\intercal$ be the vector of the state variables. In terms of the description given in (3a)-(3b), the system matrices are as follows:

$$\mathbf{A}_1 = \begin{pmatrix} -\frac{\alpha}{RC} & \frac{\alpha}{C} & 0 & 0 \\ -\frac{\alpha}{L} & -\frac{r_1}{L} & 0 & 0 \\ -\alpha k_v & -\alpha k_v r_C & -\omega_{p1} & 0 \\ -\alpha k_v & -\alpha k_v r_C & 0 & -\omega_{p2} \end{pmatrix}, \tag{28a}$$

$$\mathbf{A}_0 = \begin{pmatrix} -\frac{\alpha}{RC} & \frac{\alpha}{C} & 0 & 0 \\ -\frac{\alpha}{L} & -\frac{r_0}{L} & 0 & 0 \\ -\alpha k_v & -\alpha k_v r_C & -\omega_{p1} & 0 \\ -\alpha k_v & -\alpha k_v r_C & 0 & -\omega_{p2} \end{pmatrix}, \tag{28b}$$

$$\mathbf{B}_1 = \begin{pmatrix} -\frac{1}{C} & 0 \\ 0 & \frac{1}{L} \\ 0 & 0 \\ 0 & 0 \end{pmatrix}, \mathbf{B}_0 = \begin{pmatrix} -\frac{1}{C} & 0 \\ 0 & 0 \\ 0 & 0 \\ 0 & 0 \end{pmatrix}, \mathbf{w} = \begin{pmatrix} i_o \\ v_g \end{pmatrix}. \tag{28c}$$

According to the equivalent block diagram in Fig. 4, the control voltage can be expressed as $v_{\rm con} = W_1 v_{p1} + W_2 v_{p2} + W_i x_i$. The duty cycle d_n at the nth switching cycle can be determined as in (9) by selecting $v_r = 0$, $\rho = v_r - V_l = -V_l$, $\mathbf{K}^\intercal = (0,\ 0,\ -W_1,\ -W_2)$.

III. Predicting Subharmonic Oscillation from Reduced-Order Dynamic Models

This section bridges the gap between the different techniques for analytically deriving a closed-form mathematical expression for subharmonic oscillation boundary and show that they all lead to the same condition (1) or equivalently (2). To make the presentation easy to follow at this stage, a reduced-order model is used to illustrate the different existing approaches. The novel approach of this work will also be detailed separately in Section IV for the reduced order model and in Section V by using the full-order model.

A. Reduced-order switched continuous-time model

At this stage, let us ignore the integral action in the feedback loop ($W_i = 0$). Let us take the feedback signal $y = \mathbf{K}^\intercal\mathbf{x}$

the *only* state variable of the system while considering all the remaining state variables coincident with their averaged values (constant). According to (4a), the signal y is governed by the following differential equation:

$$\dot{y}(t) = \mathbf{K}^{\intercal}(\mathbf{m}_0(\mathbf{x}(t)) + (\mathbf{m}_1(\mathbf{x}(t)) - \mathbf{m}_0(\mathbf{x}(t)))u(t)) := m(t). \tag{29}$$

Let $m_1 = \mathbf{K}^{\intercal}\mathbf{m}_1(\mathbf{x}(t))$ and $m_0 = \mathbf{K}^{\intercal}\mathbf{m}_0(\mathbf{x}(t))$ which are the slopes of the feedback signal y during the ON and the OFF phases respectively. With a practically piecewise linear waveform of y, the slopes m_1 and m_0 are slowly varying or constant in *steady-state* regime and the right hand side of (29) can be represented in this regime by a square-wave signal $m = m_0 + (m_1 - m_0)u$ whose upper value is m_1 for $u = 1$ and lower value is m_0 for $u = 0$. The previous assumptions are widely used in the literature for analyzing the stability of the inner current loop of switching converters under peak CMC [4]–[6], [51]. Here, it is generalized for any control scheme satisfying the previous conditions. Note that under those conditions, the m-to-y transfer function is linear and according to (29) it is a simple integrator. Although strictly speaking this is an approximation for those switching converters including a filtering capacitance and a resistive load, it is also a representation of most switching converters feeding a constant voltage load such as a battery or a dc bus [52].

It should be noted that the reduced-order model given in (29) cannot predict all kinds of instabilities that could be exhibited by the system for which a full-order model is needed. If *only* subharmonic oscillation is of concern, the reduced-order model can be used to *approximately* predict the onset of this phenomenon. Different methods will be revisited below by using this reduced-order model to show the different ways to obtain (2).

B. Derivation from the time-domain discrete-time model

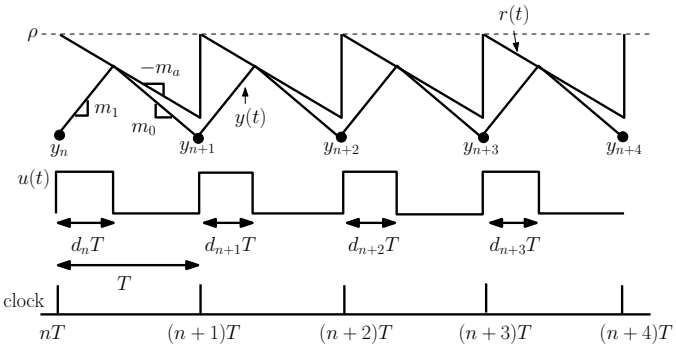

Fig. 5. The ramp signal r, the waveforms of the feedback signal y at the $T-$ periodic regime when a reduced-order model is valid.

Let $y_n = y(nT)$. By integrating (29) for the two different values of the driving signal u (Fig. 5), the discrete-time control signal y_n at time instant nT can be described by the following recurrence equation:

$$y_{n+1} = y_n + m_1 d_n T + m_0(1 - d_n)T \text{ with } 0 \leq d_n \leq 1. \tag{30}$$

For instance in peak CMC, the signal y corresponds to the controlled inductor current i_L. Note that we can make y to coincide with i_L by appropriately selecting the entries of the feedback vector $\mathbf{K}$. Namely, the component corresponding to the variable i_L will be equal to 1 while all the remaining entries in $\mathbf{K}$ will be set to 0. In general, y is a linear combination of all the state variables involved in the feedback loop. It can be demonstrated from Fig. 5 that the duty cycle d_n at the nth switching period is given by:

$$d_n = \frac{\rho - y_n}{(m_1 + m_a)T}. \tag{31}$$

The stability depends on the eigenvalue λ of the closed-loop system (30)-(31), which, in this reduced-order case, is the total derivative of y_{n+1} with respect to y_n. According to (30)-(31), the expression of λ is as follows:

$$\lambda := \frac{\mathrm{d}y_{n+1}}{\mathrm{d}y_n} = \frac{\partial y_{n+1}}{\partial y_n} + \frac{\partial y_{n+1}}{\partial d_n}\frac{\partial d_n}{\partial y_n} = \frac{m_0 + m_a}{m_1 + m_a}. \tag{32}$$

The condition for subharmonic oscillation occurrence is $\lambda = -1$ which results in (1) or equivalently (2). Note that the previous approach is equivalent to the one based on the analysis of the perturbed control signal, explained in many textbooks, research works and application notes [4]–[6].

C. Derivation from the z-domain model

The reduced-order model (30)-(31) can be decomposed into a transfer function $H(z)$ representing the power stage in the discrete-time domain consisting of a simple digital integrator (see (30)) and a PWM modulator whose $z-$domain d_n-to-y_n transfer function $F_m(z)$ can be readily obtained from (31). Therefore, the system total loop gain $\mathcal{L}(z)$ is given by:

$$\mathcal{L}(z) = \frac{m_1 - m_0}{m_1 + m_a}\frac{1}{z - 1}. \tag{33}$$

The characteristic equation of the closed loop system is $1 + \mathcal{L}(z) = 0$. The condition of an eigenvalue $\lambda = -1$ is equivalent to $1 + \mathcal{L}(-1) = 0$, i.e., $\mathcal{L}(-1) = -1$ which leads to (1) or equivalently (2).

D. Derivation from Floquet theory and Filippov method

Another way to derive the stability boundary is by using Floquet theory combined with Filippov method [27], [29]. For this technique to be applied we need the system state-space equations for the two system configurations that can be deduced from (29) by putting $u = 1$ and $u = 0$. We also need the normal η to the switching boundary defined by $\sigma := y - r = y - \rho - m_a(t \mod T) = 0$ and the time derivative $\dot{\sigma}$ of σ within a switching period T. For TEM schemes, $\eta := \partial\sigma/\partial y = 1$ and $\dot{\sigma} := \partial\sigma/\partial t = m_a$. In general, this technique gives the expression of the monodromy matrix [27], [28]. However, when applied to the reduced-order model, it gives directly the expression of the eigenvalue which can be expressed according to Filippov method as follows: $\lambda = \phi_2 S \phi_1$, where ϕ_1 and ϕ_2 are the state transition terms for the two circuit configurations and $S = 1 + (m_0 - m_1)\eta/(\eta m_1 + \dot{\sigma})$ is the saltation term due to switching at time instant DT (see [27], [28] for more details). Because the reduced-order system can be described by a simple integrator for each switch state, the state transition terms ϕ_1 and ϕ_2 are unity,

($\phi_2 = \phi_1 = 1$). Therefore, the eigenvalue of the reduced-order model coincides with the saltation term S and can be expressed as follows:

$$\lambda \equiv S = 1 + \frac{m_0 - m_1}{m_1 + m_a}. \tag{34}$$

Imposing $\lambda = -1$ in (34) also leads to (1) or equivalently (2).

IV. Approximate Prediction of Subharmonic Oscillation from the Reduced-Order Model Using the Steady-State Response

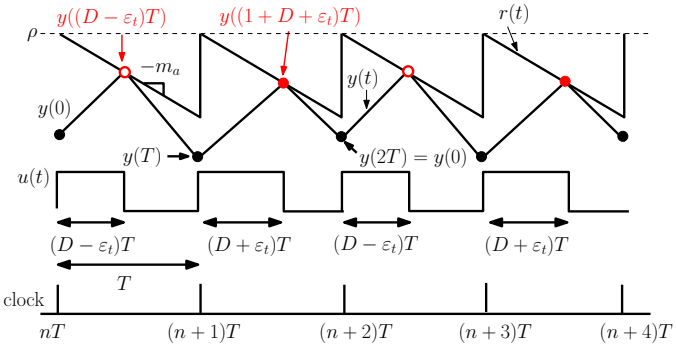

Fig. 6. The ramp signal r, steady-state waveforms of the feedback signal y and the driving signal $u(t)$ at $2T-$ periodic regime when a reduced-order model is valid.

Let D the steady-state value of the duty cycle. Since our concern is the occurrence of the first subharmonic oscillation, consider a switching regulator working under subharmonic regime with a $2T$-periodic orbit (see Fig. 6). This behavior is normally characterized by the exhibition, during two consecutive cycles in steady-state, of a narrow pulse, of duration $(D-\varepsilon_t)T$, and another wide pulse, of duration $(D+\varepsilon_t)T$, in the driving signal u and also in other square-wave signals such as the inductor voltage v_L and more specifically in the signal m. The parameter ε_t is a small quantity that vanishes at the onset of subharmonic oscillation [36], [37]. During two consecutive switching periods in the time interval $(0, 2T)$, let the crossing between the feedback signal y and the $T-$periodic signal r occurs at $t = (D-\varepsilon_t)T$ and at $t = (1+D+\varepsilon_t)T$ (see Fig. 6). From the switching conditions at these two instants, one has that:

$$y((D-\varepsilon_t)T) = \rho - m_a(D-\varepsilon_t)T, \tag{35a}$$
$$y((1+D+\varepsilon_t)T) = \rho - m_a(\not{1}+D+\varepsilon_t)T. \tag{35b}$$

Then, by subtracting (35b) from (35a), one obtains:

$$y((D-\varepsilon_t)T) - y((1+D+\varepsilon_t)T) = 2m_a\varepsilon_t T. \tag{36}$$

Like in Section III and IV, the boundary of subharmonic oscillation can be located by taking the limit in (36) when the parameter $\varepsilon_t \to 0$ [36], [37]. Therefore at the onset of this instability, the following equality holds:

$$\lim_{\varepsilon_t \to 0} \frac{1}{2\varepsilon_t T}(y((D-\varepsilon_t)T) - y((1+D+\varepsilon_t)T)) = m_a. \tag{37}$$

Different approaches can be used to obtain the steady-state response y at time instants $(D-\varepsilon_t)T$ and $(1+D+\varepsilon_t)T$ in (37) and hence to determine analytically the subharmonic oscillation boundary. Because the total loop gain of the reduced-order system is linear as explained before, linear system theory perfectly applies. The only nonlinear term responsible for subharmonic oscillation is the PWM process which is taken into account separately in (35a)-(35b) from the rest of the closed-loop system model.

A. The steady-state response from the Fourier analysis

Consider a linear time invariant system (LTI) with transfer function $H(s)$ subject to an $nT-$periodic excitation m with Fourier coefficient M_k. It is very known form linear system theory that the steady-state response y of such a system is also an $nT-$periodic signal [53, p. 228]. The relationship between the Fourier coefficients of the input and the output signals is given by [53, p. 228]:

$$Y_k = M_k H(jk\frac{2\pi}{nT}) \quad \text{for} \quad k \in \mathbb{Z}. \tag{38}$$

This is the result that was applied in [37] and used later in [33], [34], [38] for $p = 2$. The approach based on expanding the left hand side of (36) as a Fourier series using (35a)-(35b) and (38) was repeatedly called *harmonic balance* in the previous references by the same author. Exhibiting a $2T$-periodic regime, the feedback signal y can be represented by the following Fourier series:

$$y(t) = \sum_{k=-\infty}^{\infty} Y_k e^{jk\frac{\pi}{T}t}, \tag{39}$$

where Y_k is the corresponding Fourier coefficient. Then, by using (39), (37) becomes:

$$\lim_{\varepsilon_t \to 0} \sum_{k=-\infty}^{\infty} \frac{Y_k}{2T\varepsilon_t} e^{jDk\pi}((-1)^k e^{jk\pi\varepsilon_t} - e^{-jk\pi\varepsilon_t}) = m_a. \tag{40}$$

From (38), the Fourier coefficient Y_k of the feedback signal y in the $2T-$periodic regime can be written as follows:

$$Y_k = M_k H(j\frac{k\pi}{T}), \tag{41}$$

where $H(s) = 1/s$ is the m-to-y transfer function and M_k is the Fourier coefficient of the signal m at the $2T$-periodic regime which is given by:

$$M_k = \frac{1}{2T}\int_0^{2T} m(t)e^{-jk\frac{\pi}{T}t}\mathrm{d}t. \tag{42}$$

Calculating the previous integral leads to:

$$M_k = \frac{j(m_1 - m_0)}{k\pi} \times \left(-1 - (-1)^k + e^{-jDk\pi}(e^{jk\pi\varepsilon_t} + (-1)^k e^{-jk\pi\varepsilon_t}) \right), \tag{43}$$

where j is the imaginary unit and $k \neq 0$ is the harmonic order. For $k = 0$, the corresponding coefficient is $M_0 = Dm_1 + (1-D)m_0 = 0$. Then, by using (43), (40) becomes:

$$\frac{m_1 - m_0}{2\pi} \sum_{k=-\infty}^{\infty} (e^{jk2\pi D} - 1)\frac{j}{k} + \frac{j}{(k-\frac{1}{2})} = m_a. \tag{44}$$

By calculating the sum in (44), the condition for the first subharmonic oscillation occurrence becomes as follows:

$$(m_1 - m_0)(D - \frac{1}{2}) = m_a. \tag{45}$$

Because $Dm_1 + (1-D)m_0 = 0$, the previous equation also coincides with (1) or equivalently (2). One can observe that the result is obtained after going back and forth from time to frequency domains. The previous procedure can be significantly shortened by directly treating (37) in the time-domain as will be shown next.

B. Using the steady-state response directly in the time domain

Because the dynamics of the signal y is governed by a simple integrator, it can be deduced from (29) that

$$\begin{aligned} y((1+D+\varepsilon_t)T) &= y((D-\varepsilon)T) + \int_{(D-\varepsilon)T}^{(1+D+\varepsilon_t)T} m(t)\mathrm{d}t \\ &= y((D-\varepsilon)T) + m_0(1-D+\varepsilon_t)T \\ &+ m_1(D+\varepsilon_t)T. \end{aligned} \tag{46}$$

Hence, (37) becomes as follows:

$$-\lim_{\varepsilon\to 0}\frac{1}{2\varepsilon T}(m_0(1-D)T + m_1 DT + m_0\varepsilon_t T + m_1\varepsilon_t T)) = m_a. \tag{47}$$

Because $m_1 D + m_0(1-D) = 0$, (47) can be simplified as follows:

$$-\lim_{\varepsilon\to 0}\frac{1}{2\varepsilon_t T}(m_1+m_0)\varepsilon_t T = m_a \Leftrightarrow -\frac{1}{2}(m_1+m_0) = m_a, \tag{48}$$

which coincides with (2) or equivalently (1) evidencing the accuracy of the new proposed approach. Note that this direct approach in the time domain is much shorter and simpler than the one based on Fourier series expansion. Now that it is clear that all the methods lead to the same result and that only the steady-state response of the system is necessary to locate the subharmonic instability boundary, it may be concluded that there is no reason for pursuing this steady-state analysis in the frequency domain and it will be much easier to deal with the problem directly in the time domain when using a full-order model. This is what will be done in the next section for a general converter topology and control strategy.

V. A New Unified Approach for Accurate Prediction of Subharmonic Oscillations in Linear and Bilinear Switching Regulators Using the Full-Order Model

A. A unified bilinear continuous-time model for switching regulators working in CCM

The model of a dc-dc converter presented in (3a)-(3c) can also be expressed in the following general *bilinear* form:

$$\begin{aligned} \dot{\mathbf{x}}(t) &= (\mathbf{A}_1 - \mathbf{A}_0)u(t)\mathbf{x}(t) + (\mathbf{B}_1 - \mathbf{B}_0)u\mathbf{w} \\ &+ \mathbf{A}_0\mathbf{x}(t) + \mathbf{B}_0\mathbf{w}. \end{aligned} \tag{49a}$$

$$\dot{x}_i(t) = e(t). \tag{49b}$$

Note that when $\mathbf{A}_1 = \mathbf{A}_0$, the *bilinear* term $(\mathbf{A}_1 - \mathbf{A}_0)u\mathbf{x}$ vanishes and the open loop model becomes *linear*. Regardless of wether $\mathbf{A}_0 = \mathbf{A}_1$ or not, for each phase, the system equations are LTI and can be solved in closed-form. The expression of the solution $\mathbf{x}(t)$ at time t of the system starting at an initial condition $\mathbf{x}(t_0)$ at time instant t_0 takes the following form [54]:

$$\mathbf{x}(t) = e^{\mathbf{A}_u(t-t_0)}\mathbf{x}(t_0) + \int_{t_0}^{t} e^{\mathbf{A}_u(t-\tau)}\mathrm{d}\tau\mathbf{B}_u\mathbf{w}, \tag{50}$$

where $t_0 = nT$ for $u = 1$ ($t \in (nT, nT + d_nT)$) and $t_0 = nT + d_nT$ for $u = 0$ ($t \in (nT + d_nT, (n+1)T)$). The greater part of this work requires only a very moderate knowledge of nonlinear dynamics and bifurcation theory. What is chiefly required is just an understanding of the previous solution and simple matrix algebra.

Remark 1: We can compute the integral term $\int_{t_0}^{t} e^{\mathbf{A}_u(t-\tau)}\mathrm{d}\tau$ in several ways. When the state matrix $\mathbf{A}_u$ is invertible, one has the analytical formula:

$$\int_{t_0}^{t} e^{\mathbf{A}_u(t-\tau)}\mathrm{d}\tau = \mathbf{A}_u^{-1}(e^{\mathbf{A}_u(t-t_0)} - \mathbf{I}). \tag{51}$$

However, in many converter topologies, the matrix $\mathbf{A}_u$ could be singular and therefore non invertible. It should be noted that two kinds of singularities may arise in switched converters which are detailed below:

- A non structural singularity which takes place only theoretically and that can be avoided by just adding parasitic elements. This is the case, for example, of boost, buck-boost, flyback, SEPIC and Čuk converters during the charging (ON) phase. Another elegant approach to solve this type of singularity problem without adding parasitics is by using the augmented state vector technique [29], [54], [55].
- A structural singularity that cannot be avoided by just adding parasitics which arises when the system has an integral action in the feedback loop. In this case, the expression (51) cannot be used despite the fact that the integral term exists and it is well defined even in the case when the matrix $\mathbf{A}_u$ is not invertible. Having said that, in the switched model given in (3a)-(3c) or equivalently in (49a)-(49b) and the expression in (51), as it was repeatedly mentioned in this paper, the state variable corresponding to the integrator was separated from the rest of the state variables to avoid this structural singularity.

B. Steady-state response in the $T-$periodic regime

Let $\mathbf{x}(0)$ be the steady-state value of the periodic orbit of the system at the beginning of the period and $\mathbf{x}(DT)$ its value at time instant DT. Fig. 7 shows the illustrative waveforms of the $T-$periodic ramp signal r and the feedback signal $y := \mathbf{K}^\intercal\mathbf{x} - K_{vi}x_i$ when the system behavior in steady-state is $T-$periodic. Let $\mathbf{\Phi}_1 = e^{\mathbf{A}_1 DT}$, $\mathbf{\Phi}_0 = e^{\mathbf{A}_0(1-D)T}$, $\mathbf{\Psi}_1 = \int_0^{DT} e^{\mathbf{A}_1 t}\mathrm{d}t\mathbf{B}_1\mathbf{w}$ and $\mathbf{\Psi}_0 = \int_0^{(1-D)T} e^{\mathbf{A}_0 t}\mathrm{d}t\mathbf{B}_0\mathbf{w}$. The steady-state periodic orbit can be obtained by forcing that the state vector $\mathbf{x}(t_0 + T)$ after a complete switching cycle to be equal to the initial state $\mathbf{x}(t_0)$. The same applies for the

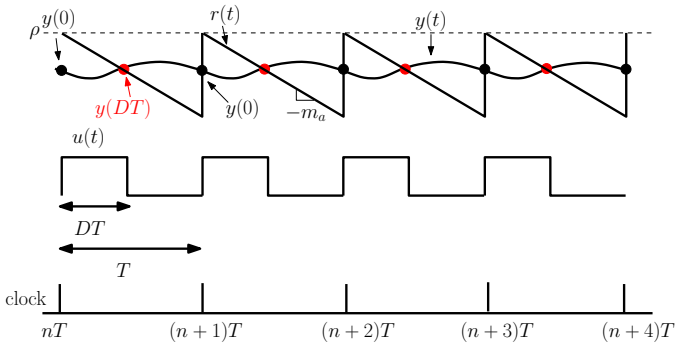

Fig. 7. The ramp signal r and steady-state waveforms of the feedback signal y at $T-$periodic regime.

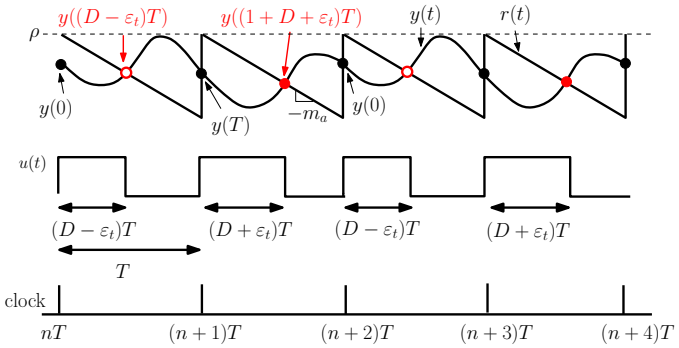

Fig. 8. The ramp signal r and steady-state waveforms of the feedback signal y at $2T-$periodic regime.

integral variable x_i. Hence, in steady-state, the vector of the non-integral state variables at the instant DT is given by:

$$\mathbf{x}(DT) = (\mathbf{I} - \mathbf{\Phi})^{-1}\mathbf{\Psi} \tag{52}$$

where $\mathbf{\Phi} = \mathbf{\Phi}_1\mathbf{\Phi}_0$ and $\mathbf{\Psi} = \mathbf{\Phi}_1\mathbf{\Psi}_0 + \mathbf{\Psi}_1$. Similarly, one can obtain that $\mathbf{x}(0)$, the value of the periodic orbit at the beginning of the switching period is as follows:

$$\mathbf{x}(0) = (\mathbf{I} - \overline{\mathbf{\Phi}})^{-1}\overline{\mathbf{\Psi}} \tag{53}$$

where $\overline{\mathbf{\Phi}} = \mathbf{\Phi}_0\mathbf{\Phi}_1$ and $\overline{\mathbf{\Psi}} = \mathbf{\Phi}_0\mathbf{\Psi}_1 + \mathbf{\Psi}_0$.

Remark 2: Because the integrator was separated from the rest of system dynamics, $\mathbf{x}(DT)$ and $\mathbf{x}(0)$ will exist and are unique whenever the matrices $\mathbf{I} - \mathbf{\Phi}$ and $\mathbf{I} - \overline{\mathbf{\Phi}}$ are invertible. This will not be the case if the integral variable was included in the vector of state variable $\mathbf{x}$ because the problem will be *ill-posed*. According to the functional analysis, the inverse of these matrices exist whenever the spectral radius of the matrices $\mathbf{\Phi}$ and $\overline{\mathbf{\Phi}}$ are less than unity [56] which is the case in all practical converter topologies since these matrices are the product of two matrix exponentials corresponding to dissipative circuit configurations.

The value of the steady-state duty cycle D is generally imposed by the voltage conversion ratio between the output and the input voltages of the converter. If there is no integral action in the loop, D must be determined by solving (in general numerically) the switching equation given in (9). In the presence of an integral variable in the feedback loop, since the steady-state value of the average controlled variable coincides with the reference signal $v_{\rm ref}$, the value of D is imposed by this reference. For instance, if the voltage to be controlled is the output voltage v_o, the steady-state value of the integral variable x_i at the final of the switching cycle can be calculated as follows:

$$x_i(T) \;=\; x_i(0) + W_i\int_0^T k_v(v_{\rm ref} - v_o(t))\mathrm{d}t. \tag{54}$$

By enforcing $T-$periodicity on $x_i(t)$, i.e., by making $x_i(0) = x_i(T)$, the following condition for the system to have periodic behavior is obtained:

$$k_vTv_{\rm ref} - k_v\int_0^T v_o(t)\mathrm{d}t \;=\; 0, \tag{55}$$

which implies that the average (dc) value V_o of the output voltage v_o is equal to the reference voltage $v_{\rm ref}$, i.e.,

$$V_o := \frac{1}{T}\int_0^T v_o(t)\mathrm{d}t = v_{\rm ref}. \tag{56}$$

Therefore, the dc value of the output voltage is uniquely determined by $v_{\rm ref}$. Since the steady-state duty cycle D in any switching converter is uniquely determined by the ratio between the average input and output voltages, there is no need to solve the switching equation given in (9) to determine D in the presence of an integral action in the output feedback loop. Once D is obtained from the voltage conversion ratio of the converter, the values of $\mathbf{x}(DT)$ and $\mathbf{x}(0)$ are straightforward from (52) and (53).

C. Steady-state response in the $2T-$ subharmonic regime

Let us consider that the system is working in subharmonic regime manifesting itself by a $2T$-periodic orbit in steady-state. Fig. 8 shows illustrative waveforms of the ramp signal r and the feedback signal y when the system behavior in steady-state is $2T-$periodic. During a switching cycle of duration $2T$, the system has four phases defined by the system matrices $(\mathbf{A}_1, \mathbf{B}_1)$, $(\mathbf{A}_0, \mathbf{B}_0)$, $(\mathbf{A}_1, \mathbf{B}_1)$ and $(\mathbf{A}_0, \mathbf{B}_0)$ respectively. Therefore, during two consecutive switching periods in the interval $(0, 2T)$, let the crossing between the signals y and r (equivalently between $v_{\rm ramp}$ and $v_{\rm con}$) occurs at $t = (D - \varepsilon_t)T$ and at $t = (1 + D + \varepsilon_t)T$. Exhibiting a $2T$-periodic regime, the sampled steady-state values of the state variables at the switching instants $(D-\varepsilon_t)T$ and $(1+D+\varepsilon_t)T$ can be obtained by using (50) and forcing $2T-$periodicity. In doing so, these values can be expressed as follows:

$$\mathbf{x}((D-\varepsilon_t)T) \;=\; (\mathbf{I} - \mathbf{\Phi}_-(\varepsilon_t))^{-1}\mathbf{\Psi}_-(\varepsilon_t), \tag{57a}$$
$$\mathbf{x}((1+D+\varepsilon_t)T) \;=\; (\mathbf{I} - \mathbf{\Phi}_+(\varepsilon_t))^{-1}\mathbf{\Psi}_+(\varepsilon_t). \tag{57b}$$

where

$$\mathbf{\Phi}_-(\varepsilon_t) \;=\; \overline{\mathbf{\Phi}}_1\overline{\mathbf{\Phi}}_4\overline{\mathbf{\Phi}}_3\overline{\mathbf{\Phi}}_2, \tag{58a}$$
$$\mathbf{\Phi}_+(\varepsilon_t) \;=\; \overline{\mathbf{\Phi}}_3\overline{\mathbf{\Phi}}_2\overline{\mathbf{\Phi}}_1\overline{\mathbf{\Phi}}_4 \tag{58b}$$
$$\mathbf{\Psi}_-(\varepsilon_t) \;=\; \overline{\mathbf{\Phi}}_1\overline{\mathbf{\Phi}}_4\overline{\mathbf{\Phi}}_3\overline{\mathbf{\Psi}}_2 + \overline{\mathbf{\Phi}}_1\overline{\mathbf{\Phi}}_4\overline{\mathbf{\Psi}}_3 + \overline{\mathbf{\Phi}}_1\overline{\mathbf{\Psi}}_4 + \overline{\mathbf{\Psi}}_1 \tag{58c}$$
$$\mathbf{\Psi}_+(\varepsilon_t) \;=\; \overline{\mathbf{\Phi}}_3\overline{\mathbf{\Phi}}_2\overline{\mathbf{\Phi}}_1\overline{\mathbf{\Psi}}_4 + \overline{\mathbf{\Phi}}_3\overline{\mathbf{\Phi}}_2\overline{\mathbf{\Psi}}_1 + \overline{\mathbf{\Phi}}_3\overline{\mathbf{\Psi}}_2 + \overline{\mathbf{\Psi}}_3 \tag{58d}$$

and

$$\overline{\mathbf{\Phi}}_1 = \mathbf{\Phi}_1 e^{-\mathbf{A}_1\varepsilon_t T},\ \overline{\mathbf{\Psi}}_1 = \int_0^{(D-\varepsilon_t)T} e^{\mathbf{A}_1\tau}\mathrm{d}\tau\mathbf{B}_1\mathbf{w} \quad (59a)$$

$$\overline{\mathbf{\Phi}}_2 = \mathbf{\Phi}_0 e^{\mathbf{A}_0\varepsilon_t T},\ \overline{\mathbf{\Psi}}_2 = \int_0^{(1-D+\varepsilon_t)T} e^{\mathbf{A}_0\tau}\mathrm{d}\tau\mathbf{B}_0\mathbf{w} \quad (59b)$$

$$\overline{\mathbf{\Phi}}_3 = \mathbf{\Phi}_1 e^{\mathbf{A}_1\varepsilon_t T},\ \overline{\mathbf{\Psi}}_3 = \int_0^{(D+\varepsilon_t)T} e^{\mathbf{A}_1\tau}\mathrm{d}\tau\mathbf{B}_1\mathbf{w} \quad (59c)$$

$$\overline{\mathbf{\Phi}}_4 = \mathbf{\Phi}_0 e^{-\mathbf{A}_0\varepsilon T},\ \overline{\mathbf{\Psi}}_4 = \int_0^{(1-D-\varepsilon_t)T} e^{\mathbf{A}_0\tau}\mathrm{d}\tau\mathbf{B}_0\mathbf{w} \quad (59d)$$

D. A direct time-domain derivation of subharmonic oscillation boundary

Let $r^- = ((D-\varepsilon_t)T)$ and $r^+ = ((D+\varepsilon_t)T)$ From the switching conditions at time instants $(D-\varepsilon_t)T$ and $(1+D+\varepsilon_t)T$, imposed by the control mode and the modulation strategy, the following equalities hold (see Fig. 8):

$$\mathbf{K}^\intercal\mathbf{x}((D-\varepsilon_t)T) - W_i x_i((D-\varepsilon_t)T) = r^- \quad (60a)$$

$$\mathbf{K}^\intercal\mathbf{x}((1+D+\varepsilon_t)T) - W_i x_i((1+D+\varepsilon_t)T) = r^+ \quad (60b)$$

Subtracting (60b) from (60a), one obtains:

$$\begin{aligned}\mathbf{K}^\intercal(\mathbf{x}((D-\varepsilon_t)T) &- \mathbf{x}((1+D+\varepsilon_t)T)\\ &- W_i x_i((1+D+\varepsilon_t)T)\\ &- W_i x_i((D-\varepsilon_t)T) = 2m_a\varepsilon_t T \quad (61)\end{aligned}$$

While in [33], [34], [37], the previous equation is expressed in the Fourier domain only for ideal buck converters for which one has $\mathbf{A}_1 = \mathbf{A}_0$ without showing the explicit dependence on the integral term, in this paper this equation is directly treated in the time-domain for the general case of bilinear converters characterized by $\mathbf{A}_1 \neq \mathbf{A}_0$ without any extra effort to go back from the Fourier frequency-domain into the time-domain and by explicitly evincing the effect of the integral action in the feedback loop. Like in section IV, the The boundary of subharmonic oscillation can be located by taking the limit in (61) when the parameter $\varepsilon_t \to 0$. Therefore at the onset of this instability, the following equality holds:

$$m_P + m_I = m_a, \quad (62)$$

where the terms m_P and m_I are two limits given by:

$$m_P = \mathbf{K}^\intercal \lim_{\varepsilon_t\to 0} \frac{\mathbf{x}((D-\varepsilon_t)T) - \mathbf{x}((1+D+\varepsilon_t)T)}{2\varepsilon_t T}, \quad (63a)$$

$$m_I = -W_i \lim_{\varepsilon_t\to 0} \frac{x_i((D-\varepsilon_t)T) - x_i((1+D+\varepsilon_t)T)}{2\varepsilon_t T}. \quad (63b)$$

Because the state equations of the integral variable x_i is a simple integrator, the expression of $x_i((1+D+\varepsilon_t)T)$ in steady-state is as follows:

$$x_i((1+D+\varepsilon_t)T) = x_i((D-\varepsilon_t)T) + \int_{(D-\varepsilon_t)T}^{(1+D+\varepsilon_t)T} e(t)\mathrm{d}t. \quad (64)$$

At the boundary between periodic and subharmonic regime, the integral of the error voltage during one complete period of length T is zero as demonstrated in (55). Therefore, the term m_I is given by:

$$m_I = W_i \lim_{\varepsilon_t\to 0} \frac{1}{2\varepsilon_t T} \int_{(D-\varepsilon_t)T}^{(1+D+\varepsilon_t)T} e(t)\mathrm{d}t. \quad (65)$$

This term, which shows the effect of the integral action on the subharmonic oscillation boundary, is straightforward from (65) and can be expressed as follows:

$$m_I = W_i e(DT). \quad (66)$$

On the other hand, by using (57b)-(57a), the term m_P in (63a) becomes:

$$m_P = -\lim_{\varepsilon_t\to 0} \frac{(\mathbf{I}-\mathbf{\Phi}_+)^{-1}\mathbf{\Psi}_+ - (\mathbf{I}-\mathbf{\Phi}_-)^{-1}\mathbf{\Psi}_-}{2\varepsilon_t T}. \quad (67)$$

where dependence on ε_t has been omitted in the expressions of $\mathbf{\Phi}_+$ and $\mathbf{\Phi}_-$ for simplicity. Following the same procedure of [57], m_P can be derived by calculating the limit in (67) hence obtaining:

$$m_P = -\mathbf{K}^\intercal(\mathbf{I}+\mathbf{\Phi})^{-1}\mathbf{\Phi}_1(\mathbf{m}_1(\mathbf{x}(0)) + \mathbf{m}_0(\mathbf{x}(0))), \quad (68)$$

and finally the subharmonic oscillation boundary in (62) taking into account the integral action in the feedback loop can expressed as follows:

$$-\mathbf{K}^\intercal(\mathbf{I}+\mathbf{\Phi})^{-1}\mathbf{\Phi}_1(\mathbf{m}_1(\mathbf{x}(0))+\mathbf{m}_0(\mathbf{x}(0))) + W_i e(DT) = m_a. \quad (69)$$

Hence, if subharmonic oscillation is of concern, the procedure to obtain its boundary from (69) can be summarized as follows: (i) represent the regulator (power stage and compensator) using a state-space model as in (3a)-(3c) and identify the linear vector fields $\mathbf{m}_1$ and $\mathbf{m}_0$, (ii) obtain the steady-state values $\mathbf{x}(DT)$ and $\mathbf{x}(0)$ from (52) and (53) respectively, (iii) use the control strategy to identify the vector of the feedback coefficients $\mathbf{K}$, (iv) evaluate the subharmonic condition (69) and plot the critical curve in terms of suitable parameters. Note that all the steps in the previous procedure are analytical except the evaluation of the matrix exponentials which could require a numerical computation. The value of the matrix exponential can be found analytically only for low dimensional cases. Analytical computation of the matrix exponentials will lead to cumbersome expressions even for a two-dimensional case. However, it is much better from a practical point of view to have a simple analytical expression than to solve the entire problem numerically. Moreover, to gain more insights, approximations can be performed under some practical conditions and the results can be interpreted using slope-based or ripple-based criteria as in [46]. In part II of this paper, the procedure for plotting the subharmonic oscillation boundary in a practical example of switching regulator will be illustrated using a MATLAB© code where the matrix exponentials are computed by the function `expm` which uses a scaling and squaring algorithm.

Remark 3: The subharmonic oscillation condition in (69) is expressed in terms of the compensating ramp slope m_a. However, it can also be interpreted in terms of many other parameters as will be detailed in Part II of this paper. The results can also be adapted for all LEM strategies by simply

changing the steady-state duty cycle D by its complementary $1-D$.

It is worth mentioning here that in [32], a differently expressed condition was obtained using a *dynamic* approach based on solving the eigenvalue problem of the characteristic equation for the same boundary condition. Although they are expressed differently, the critical ramp slope for subharmonic oscillation given in (69) and the one derived in [32] are coincident. However, differently to [32], the effect of the integral action is explicitly shown in the new expression (69).

Remark 4: While it was conjectured in [28] that the integral action has no effect on the subharmonic oscillation boundary, (69) shows that this will be the case only when $m_I = 0$, i.e, $e(DT) = 0$. It turns out that in the buck converter under VMC considered in [28], the error voltage at time instant DT is very small ($e(DT) = k_v(v_{\rm ref} - v_o(DT) = v_{\rm ref} - v(DT)) \approx 0$) making the term m_I negligible in front of m_P and effectively the integral term has very little effect on the subharmonic oscillation boundary in this case. In general, the integral term corresponding to voltage feedback can be neglected in any practical converter. In fact, it can be demonstrated that the upper bounds of the terms $e(DT)$ are the $T-$periodic ripple amplitude of the controlled variable, i.e., $e(DT) < \Delta i_L$ and $e(DT) < \Delta v_o$, (Fig. 9). Without loss of generality, let $k_v = 1$. The voltage ripple is very small in any practical design (less than 1%) and its corresponding term $W_i e(DT)$ could be neglected without a significant alteration of the results as will be shown in Part II of this paper using different case studies. This is not the case when $W_i e(DT)$ corresponds to current integrator because the term $e(DT)$ almost coincides with the current ripple amplitude Δi_L (Fig. 9(e) and Fig. 9(f)) which could be significant in practical switching converters (up to 30%). Therefore, while in VMC, the integral action can be ignored for predicting subharmonic oscillation, the integral action in the current loop could have a significant effect on this phenomenon [58]. Note that when the output voltage is discontinuous at the switching instants due to parasitic parameters such as in the boost converter with an ESR (Fig. 9(d)) or in the buck converter with an ESL in the output capacitor (Fig. 9(c)), the ripple must still be maintained at very low values and hence the corresponding integral term m_I can also be ignored in these cases. This is also the case when the output voltage ripple have a triangular shape such as in ripple-based control methods in buck converters with a dominant ripple due to the ESR of the output capacitor (Fig. 9(b)).

Remark 5: In the presence of a small propagation delay δT ($\delta < D$), the same condition (69) is still valid by multiplying its left hand side by $e^{-\mathbf{A}_1 \delta T}$ and replacing $e(DT)$ by $e((D-\delta)T)$. The previous considerations in Remark 4 also apply in the presence of such a propagation delay.

VI. Conclusions, contributions, extension to other instabilities and control schemes

Subharmonic instability boundaries of switching converters in terms of the system parameters can be used for design purposes in order to guarantee a stable periodic regime and satisfactory performances. Power electronics designers have traditionally used approximated design-oriented expressions for such boundaries. In this part of the paper a direct static approach was presented for the accurate prediction of this phenomenon obtaining a simple closed-form condition. Hence, the effect of the different parameters of the system upon the steady-state behavior can be unveiled. The simple expression was derived without the need of the Jacobian matrix and without expressing the system trajectories in the Fourier frequency-domain. The general-purpose derived expression can be applied to different examples of PWM converters under different modulation strategies and control modes and is not limited to those converters characterized by a linear power stage. Therefore, the method presented here generalizes the recently reported results in [33], [34], [38] to bilinear switching converters. Yet, the new simple static approach used in this paper mathematically shows that an appropriate analysis of the steady-state response in the time domain can be used to obtain the boundary of subharmonic oscillation in switching converters with both linear and bilinear power stages. In contrast to previous studies, the effect of the integral action in the feedback loop was explicitly revealed. The proposed approach separates the integral state variable from the power stage and other state variables in the controller. Whilst this arrangement is consistent with the fact that the integral variable converges to a steady-state value only once the corresponding loop is closed, the implied dynamics separation between this variable and the rest of state variables resulted on revealing clearly the effect of the integral action on the subharmonic oscillation boundary while allowing to start the approach with a *well-posed* problem. The derived expression is dependent upon the system state transition matrices and different power stages and control strategies could be evaluated by suitably specifying the respective system matrices and feedback coefficients. The derived expression can be used as an off-line tool to evaluate the stability boundary in switching converters.

The contributions of this work are as follows:

- The work demonstrated that a careful analysis of the system steady-state orbit in the time domain can be used to derive an exact critical condition for subharmonic oscillation occurrence in switching converters. A new exact matrix-form expression was obtained for that purpose without needing to calculate the Jacobian matrix or to expand the state variables in a Fourier series.
- The effect of the integral action in the feedback loop on the subharmonic oscillation was explicitly revealed.

As supported by different case studies considered in Part II [59], the derived expression can accurately predict the onset of subharmonic oscillation in switching converters under all fixed frequency control strategies. It should also be noted that although the focus of this work is on subharmonic oscillation boundary, (69) can be easily adjusted to predict saddle-node bifurcation by just changing the sum $\mathbf{m}_1(\mathbf{x}(0)) + \mathbf{m}_0(\mathbf{x}(0))$ by the difference $\mathbf{m}_1(\mathbf{x}(0)) - \mathbf{m}_0(\mathbf{x}(0))$ and the sum $\mathbf{I} + \mathbf{\Phi}$ by the difference $\mathbf{I} - \mathbf{\Phi}$. More details are in [57], [60], [61]. The method presented in this study can also be easily adapted to deal with switching converters under variable frequency

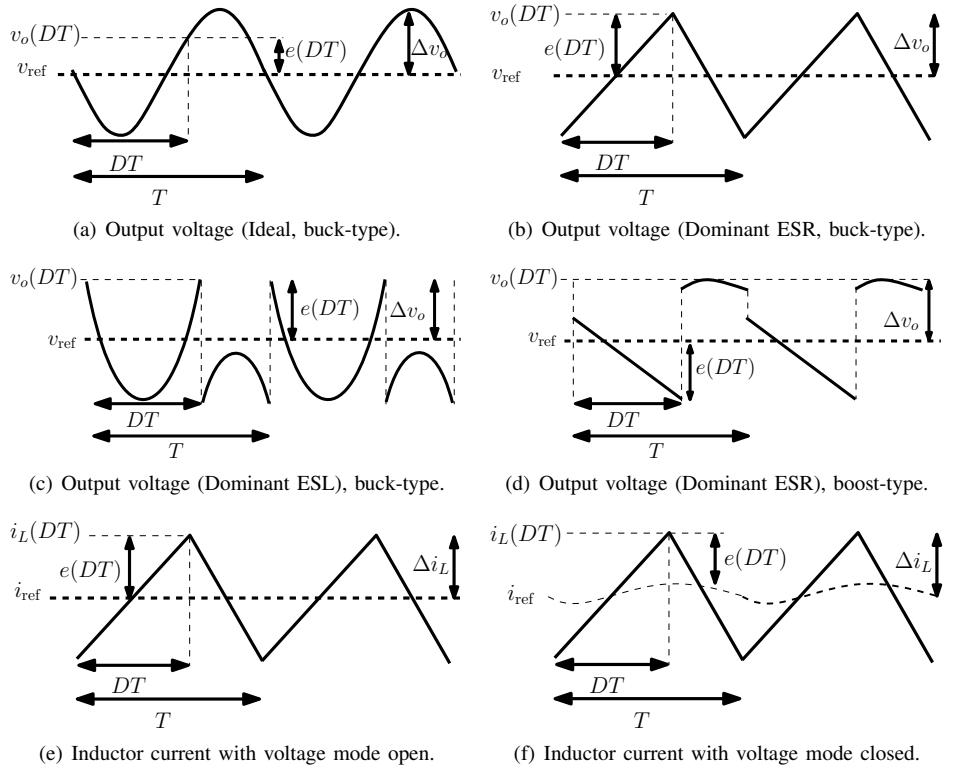

(a) Output voltage (Ideal, buck-type).

(b) Output voltage (Dominant ESR, buck-type).

(c) Output voltage (Dominant ESL), buck-type.

(d) Output voltage (Dominant ESR), boost-type.

(e) Inductor current with voltage mode open.

(f) Inductor current with voltage mode closed.

Fig. 9. Illustrative waveforms of the output voltage ripple (a, b, c and d) and the inductor current of a switching converter (e,f). (a) curved waveforms that could represent the output voltage of a buck converter with ideal capacitor. (b) piecewise linear but continuous waveform representing the output voltage of a buck converter with dominant ripple due to ESR of the capacitor. (c) discontinuous output voltage ESL in the buck converter. (d) discontinuous output voltage due to ESR of the capacitor in the boost converter. (e) inductor current of a switching converter and its fixed reference (with voltage loop open). (f) inductor current of a switching converter and its reference dictated by the outer voltage loop (with voltage loop closed).

control strategies such as constant ON time and constant OFF time schemes.

REFERENCES

[1] R. Redl and I. Novak, "Instabilities in current-mode controlled switching voltage regulators," in *IEEE Power Electronics Specialists Conference (PESC'81)*, 1981, pp. 17–28.

[2] B. Holland,"Modelling, analysis and compensation of the current-mode converter", *Proc. Powercon,* vol. 11, no. I2-1-I-2-6, 1984.

[3] R. B. Ridley, "A new continuous-time model for current-mode control," *IEEE Transactions on Power Electronics*, vol.6, no. 2, pp. 271-282, 1991.

[4] S. W Lee, "Practical feedback loop analysis for current-mode boost converter, Texas Instruments, Application Report SLVA636-March 2014, available online.

[5] R. W. Erickson and D. Maksimovic, *Fundamentals of power electronics*. Lluwer, Springuer, 2001.

[6] I. Zafrany, S. Ben-Yaakov, "A chaos model of subharmonic oscillations in current mode PWM boost converters," *Eighteenth Convention of Electrical and Electronics Engineers in Israel,* 1995., pp. 5.4.5/1, 5.4.5/5, 7-8, 1995.

[7] B. Bao, G. Zhou J. Xu; Z. Liu, "Unified classification of operation-state regions for switching converters with ramp compensation," *IEEE Transactions on Power Electronics,* vol. 26, no. 7, pp. 1968-1975, 2011.

[8] A. El Aroudi, "Prediction of subharmonic oscillation in switching converters under different control strategies," *IEEE Transactions on Circuits and Systems II: Express Briefs*, vol. 62, no. 11, pp-910-914, 2014.

[9] A. El Aroudi, J. Calvente, R. Giral, R., M. Al-Numay, and L. Martinez-Salamero, "Boundaries of subharmonic oscillations associated to filtering effects of controllers and current sensors in switched converters under CMC", *IEEE Transactions on Industrial Electronics,*, vol. 63, no. 8, pp. 4826-4837, 2016.

[10] A. V. Anunciada, M. M. Silva, "On the stability and subharmonic susceptibility of current-mode controlled converters," *23rd Annual IEEE Power Electronics Specialists Conference, 1992.* PESC '92 Record., pp. 345-353 vol. 1, 1992.

[11] Y. Yingyi, F.C. Lee, P. Mattavelli, "Analysis and design of average current mode control using a describing-function-based equivalent circuit model," *IEEE Transactions on Power Electronics,* vol. 28, no. 10, pp.4732-4741, 2013.

[12] J. Li and F. C. Lee, "Modeling of V^2 current-mode control," *IEEE Transactions on Circuits and Systems-I: Regular Papers,* vol. 57, no. 9, pp. 2552-2563, 2010.

[13] J. Li and F. Lee, "New modeling approach and equivalent circuit representation for current-mode control," *IEEE Transactions on Power Electronics,* vol. 25, no. 5, pp. 1218-1230, 2010.

[14] J. H. B. Deane and D. C. Hamill, "Instability, subharmonics, and chaos in power electronic systems," *IEEE Transactions on Power Electronics,* vol. 5, no. 2, pp. 260-268, 1990.

[15] D. C. Hamill, J. H. B. Deane, and D. Jefferies, "Modeling of chaotic DC-DC converters by iterated nonlinear mappings," *IEEE Transactions on Power Electronics,* vol. 7, no. 1, pp. 25-36, 1992.

[16] C. K. Tse and W. C. Y. Chan, "Chaos from a current-programmed Cuk converter," *International Journal Circuit Theory and Applications,* vol. 23, no. 3, pp. 217-225, 1995.

[17] E. Fossas and G. Olivar "Study of chaos in the buck converter," *IEEE Transactions on Circuits and Systems I: Fundamental Theory and Applications*, vol. 43, no. 1, pp. 13–25, 1996.

[18] C. K. Tse, S. C. Fung, and M. W. Kwan, "Experimental confirmation of chaos in a current-programmed Čuk converter," *IEEE Transactions on Circuits and Systems I: Theory and Applications,* vol. 43, no. 7, pp. 605-608, 1996.

[19] K. Chakrabarty, G. Poddar, and S. Banerjee, "Bifurcation behavior of the buck converter," *IEEE Transactions on Power Electronics,* vol. 11, no. 3, pp. 439-447, 1996.

[20] S. Banerjee and K. Chakrabarty, "Nonlinear modeling and bifurcation in the boost converter," *IEEE Transactions on Power Electronics,* vol. 13, no. 2, pp. 252-260, 1998.

[21] M. di Bernardo, F. Vasca, "Discrete-time maps for the analysis of bifurcations and chaos in DC/DC converters," *IEEE Transactions on Circuits and Systems I: Fundamental Theory and Applications*, vol. 47, no. 2, pp. 130–143, 2000.

[22] S. K. Mazumder, A. H. Nayfeh, D. Boroyevich, "Theoretical and experimental investigation of the fast- and slow-scale instabilities of a DC-DC converter," *IEEE Transactions on Power Electronics,* vol. 16, no. 2, pp. 201-216, 2001.

[23] C.K. Tse, Complex Behavior of Switching Power Converters, Boca Raton, USA: CRC Press, 2003.

[24] G. A. Papafotiou, N. I. Margaris, "Calculation and stability investigation of periodic steady states of the voltage controlled Buck DC-DC converter," *IEEE Transactions on Power Electronics,* vol. 19, no. 4, pp. 959-970, 2004.

[25] R. Gavagsaz-Ghoachani, J.-P Martin, S. Pierfederici, B. Nahid-Mobarakeh, B. Davat, "DC Power Networks With Very Low Capacitances for Transportaion Systems: Dynamic Behavior Analysis," *IEEE Transactions on Power Electronics,* vol. 28, no. 12, pp. 5865-5877, 2013.

[26] R. Gavagsaz-Ghoachani M. Phattanasak J.-P. Martin S. Pierfederici B. Nahid-Mobarakeh and B. Davat, "Generalisation of an averaged model approach to estimate the period-doubling bifurcation onset in power converters," *IET Power Electronics*, vol. 9, no. 5, pp. 977-988, 2016.

[27] D. Giaouris, S. Banerjee, B. Zahawi, V. Pickert, "Stability analysis of the continuous-conduction-mode buck converter via Filippov's method," *IEEE Transactions on Circuits and Systems I: Regular Papers,* vol. 55, no. 4, pp. 1084-1096, 2008.

[28] D. Giaouris, S. Maity, S. Banerjee, V. Pickert, and B. Zahawi, "Application of Filippov method for the analysis of subharmonic instability in DC-DC converters," *International Journal of Circuit Theory and Applications*, vol. 37, no. 8, pp. 899-919, 2009.

[29] J. Cortes, V. Svikovic, P. Alou, J. A. Oliver, J. A. Cobos, R. Wisniewski, "Accurate analysis of subharmonic oscillations of V^2 and $V^2 I_c$ controls applied to buck converter," *IEEE Transactions on Power Electronics,* vol. 30, no. 2, pp. 1005-1018, 2015.

[30] A. Shahin, R. Gavagsaz-Ghoachani, J.-P Martin, S. Pierfederici, Davat, B. F. Meibody-Tabar, "New method to filter HF current ripples generated by current-fed DC/DC converters," *IEEE Transactions on Power Electronics,* vol. 26, no. 12, pp. 3832-3842, 2011.

[31] R. Gavagsaz-Ghoachani, J. Martin, S. Pierfederici, B. Nahid-Mobarakeh, B. Davat, B., "DC Power networks with very low capacitances for transportation systems: Dynamic behavior analysis," *IEEE Transactions on Power Electronics,* vol. 28, no. 12, pp. 5865-5877, 2013.

[32] C.-C. Fang, "Instability conditions for a class of switched linear systems with switching delays based on sampled-data analysis: applications to DC-DC converters," *Nonlinear Dynamics,* vol. 77, no. 1-2, pp. 185-208, 2014.

[33] C.-C. Fang, "Closed-Form critical conditions of subharmonic oscillations for buck converters," *IEEE Transactions on Circuits and Systems I: Regular Papers,* vol. 60, no. 7, pp. 1967-1974, 2013.

[34] C.-C. Fang and R. Redl, "Subharmonic instability limits for the peak-current-controlled buck converter with closed voltage feedback loop," *IEEE Transactions on Power Electronics* vol. 30, no. 2, pp. 1085-1092, 2015.

[35] R. Gavagsaz-Ghoachani, M. Phattanasak, J.-P. Martin, S. Pierfederici, B. Davat, "Predicting the onset of bifurcation and stability study of a hybrid current controller for a boost converter,"*Mathematics and Computers in Simulation,* vol. 91, pp. 262-273, 2013.

[36] C.-C. Fang, "Sampled-data analysis and control of DC-DC switching converters." PhD thesis, Dept. of Elect. Eng., Univ. of Maryland, College Park, 1997.

[37] C.-C. Fang and E. H. Abed, "Harmonic balance analysis and control of period doubling bifurcation in buck converters," in *IEEE International Symposium on Circuits and System*, vol. 3, pp. 209–212, 2001.

[38] C.-C. Fang and C.-J. Chen, "Subharmonic instability limits for V^2-controlled buck converter with outer loop closed/open," *IEEE Transactions on Power Electronics,* vol. 31, no. 2, pp. 1657-1664, 2015.

[39] J. Cortes, V. Svikovic, P. Alou, J. Oliver, J. A. Cobos, "V^1 concept: designing a voltage mode control as current mode with near time-optimal response for Buck-type converters," *IEEE Transactions on Power Electronics,* vol. 30, no. 10, pp. 5829-5841, 2015.

[40] Y. Yan, F. Lee, P. Mattavelli, and P.-H. Liu, "I^2 average current mode control for switching converters," *IEEE Transactions on Power Electronics,* vol. 29, no. 4, pp. 2027-2036, 2014.

[41] C.-C. Fang, "Prediction of subharmonic oscillation in I^2 controlled buck converters in CCM," *IEEE Transactions Power Electronics,* vol. 30, no. 7, pp. 4035-4036, 2015.

[42] Y. Yan, F. V. Lee, and P. Mattavelli, "Unified three-terminal switch model for current mode controls," *IEEE Transactions on Power Electronics*, vol. 27, no. 9, pp. 4060-4070, 2012.

[43] W. Xiao; W. G. Dunford, P. R. Palmer, A. Capel, "Regulation of photovoltaic voltage," *IEEE Transactions on Industrial Electronics,* vol. 54, no. 3, pp. 1365-1374, 2007.

[44] M.-G. Kim, "Error amplifier design of peak current controlled (PCC) buck LED driver," *IEEE Transactions on Power Electronics,* vol. 29, no. 12, pp. 6789-6795, 2014.

[45] M.-G Kim, "Proportional-Integral (PI) compensator design of duty-cycle-controlled buck LED driver," *IEEE Transactions on Power Electronics,* vol. 30, no. 7, pp. 3852-3859, 2015.

[46] A. El Aroudi, M. Al-Numay, J. Calvente, R. Giral, E. Rodriguez and E. Alarcón, "Prediction of subharmonic oscillation in switching regulators: From a slope to a ripple standpoint," *International Journal of Electronics*, doi:10.1080/00207217.2016.1178342, in press, 2016.

[47] R. D. Middlebrook, "Modeling Current-Programmed Buck and Boost Regulators, *IEEE Transactions on Power Electronics,* vol. 4, no. 1, pp. 36-52, 1989.

[48] A. El Aroudi, K. Mandal, D. Giaouris, S. Banerjee, A. Abusorrah, Al M. Hindawi, and Y. Al-Turki, "Fast-scale stability limits of a two-stage boost power converter," *International Journal of Circuit Theory and Applications,* vol. 44, no. 5, pp. 1127-1141, 2016.

[49] A. El Aroudi, D. Giaouris, K. Mandal, S. Banerjee, M. Al Hindawi, A. Abusorrah, and Y. Al-Turki, "Complex non-linear phenomena and stability analysis of interconnected power converters used in distributed power systems," *IET Power Electronics,* vol. 9, no. 5, pp. 855-863, 2016.

[50] Intersil, "Designing stable compensation networks for single phase voltage mode buck regulators," Technical Brief TB417.1. [Online]. Available: http://www.intersil. com/content/dam/Intersil/documents/tb41/tb417.pdf

[51] T. Kabe, S. Parui, H. Torikai, S. Banerjee and T. Saito, "Analysis of piecewise constant models of curent mode controlled DC-DC converters," *IEICE Transactions on Fundamentals of Electronics, Communication and Computer Sciences*, E90-A(2), 2007, pp. 448-456.

[52] A. Costabeber, M. Carraro, M. Zigliotto, "Convergence analysis and tuning of a sliding-mode ripple-correlation MPPT," *IEEE Transactions on Energy Conversion,* vol. 30, no. 2, pp. 696-706, 2015.

[53] A. V. Oppenheim, A. S. Willsky, N. Hamid S. Hamid, "Signals and systems," Pearson Education, 1998.

[54] K. J. Aström and B. Wittenmark. "Computer-control systems: Theory and design," Prentice Hall, Englewood Cliffs, NJ, 3rd edition, 1997.

[55] H. R. Visser, P. P. J. van den Bosch, "Modelling of periodically switching networks," *22nd Annual IEEE , Power Electronics Specialists Conference,* PESC'91 Record., pp. 67-73, 24-27 Jun 1991.

[56] N. Suzuki, "On the convergence of Neumann series in Banach space," *Mathematische Annalen,* vol. 220, no. 2, pp. 143-146, 1976.

[57] A. El Aroudi, "A Time-domain asymptotic approach to predict saddle-node and period doubling bifurcations in pulse width modulated piecewise linear systems," The *International Conference on Structural Nonlinear Dynamics and Diagnosis*, Agadir, Morocco, 2014.

[58] A. E. Aroudi, "Prediction of subharmonic oscillation in switching regulators with integrative feedback loops," 2016 IEEE *International Symposium on Circuits and Systems* (ISCAS), Montreal, QC, 2016, pp. 441-444.

[59] A. El Aroudi, "A new approach for accurate prediction of subharmonic oscillation in switching regulators–Part II: Case studies," *IEEE Transactions on Power Electronics*, submitted, 2016.

[60] A. El Aroudi, M. Al-Numay, K. Al Hosani and N. Al Sayari, "Using Steady-State Response for Predicting Stability Boundaries in Switched Systems Under PWM with Linear nd Bilinear Plants", in *Structural Nonlinear Dynamics and Diagnosis*, pp. 367-391, Springer, 2015.

[61] A. El Aroudi, D. Giaouris, H. H. C. Iu and I. Hiskens, "A review on stability analysis methods for switching mode power converters", *IEEE Journal on Emerging Topics on Circuits and Systems*, vol.5, no.3, pp. 302-315, 2015.

Abdelali El Aroudi (M'00, SM'13) received the graduate degree in physical science from Facult´e des sciences, Université Abdelmalek Essaadi, Tetouan, Morocco, in 1995, and the Ph.D. degree (hons) in applied physical science from Universitat Polit'ecnica de Catalunya, Barcelona, Spain in 2000. During the period 1999-2001 he was a Visiting Professor at the Department of Electronics, Electrical Engineering and Automatic Control, Technical School of Universitat Rovira i Virgili (URV), Tarragona, Spain, where he became an associate professor in 2001 and a full-time tenure Associate Professor in 2005. From September 2007 to January 2008 he was holding a visiting scholarship at the Department of Mathematics and Statistics, Universidad Nacional de Colombia, Manizales, conducting research on modeling of power Electronics circuits for energy management. From February 2008 to July 2008, he was a visiting scholar at the Centre de Recherche en Sciences et Technologies de Communications et de l´Informations (CReSTIC), Reims, France. From September 2014 to December 2014, he was a visiting scholar at Institut National des Sciences Appliquées (INSA), Université of Toulouse, France and the Laboratoire d'Analyse et d'Architecture des Systèmes (LAAS) of the Centre National de la Recherche Scientifique (CNRS), Toulouse, France. From January 2015 to July 2015, he was a visiting professor at The Petroleum Institute, Abu Dhabi, UAE. His research interests are in the field of structure and control of power conditioning systems for autonomous systems, power factor correction, stability problems, nonlinear phenomena, chaotic dynamics, bifurcations and control. He is a Guest Editor of the IEEE Journal on Emerging and Selected Topics in Circuits and Systems Special Issue on Design of Energy-Efficient Distributed Power Generation Systems (September 2015). He currently serves as Associate Editor in *IEE IET Power Electronics* and *IEE IET Electronics Letters.*